

Monte-Carlo simulations of light propagation in luminescent solar concentrators based on semiconductor nanoparticles

Derya Şahin, Boaz Ilan,^{a)} and David F. Kelley

School of Natural Sciences, University of California, Merced, California 95343, USA

(Received 6 April 2011; accepted 25 June 2011; published online 11 August 2011)

Semiconductor nanoparticles have a wide absorption band and small reabsorption probability, which makes them great candidates for luminescent solar concentrators (LSCs). We use Monte-Carlo simulations of photon transport to predict the performance of LSCs based on “type-II” CdSe-CdTe quantum dots. These computations suggest that semiconductor-based LSCs can be highly efficient. The optimum performance is reached with a fairly long LSC with a photovoltaic cell covering only one edge. In addition, when the LSC has CdSe-CdTe nanorods that are aligned perpendicular to the top surface, the escape of photons from the top surface is significantly reduced. These results are encouraging for cost-effective LSC designs based on semiconductor nanoparticles. © 2011 American Institute of Physics. [doi:10.1063/1.3619809]

I. INTRODUCTION

Photovoltaic (PV) solar cells have become much more efficient over the past few decades, yet remain fairly expensive compared with competing energy sources. Since the 1970s, researchers have been developing luminescent solar concentrators (LSCs),^{1–4} which can concentrate light to a small PV cell at the edge of the device (see Fig. 1). Unlike other types of solar concentrators, which can only concentrate direct (specular) light, LSCs can also absorb and concentrate diffuse light. One of the key ideas in using LSCs is for fluorescent particles to absorb and reemit light at longer wavelengths, which can be more efficiently converted to electricity by a PV cell. To achieve this, most current LSCs rely on luminescent small-molecule dyes or organic polymer dyes,^{5–10} whose performance has been considerably improved over the past two decades. A more recent approach is the usage of semiconductor nanoparticles, thus far, mostly of “type-I” (commonly based on CdSe or PbSe).^{11–14} Unfortunately, neither approach has yielded LSCs that are efficient enough to be cost effective. Both approaches suffer from the same fundamental limitation: to absorb more sunlight the concentration of the active media needs to be high, but with a higher concentration the luminescence is more likely to be reabsorbed. The performance of the LSC is then limited by the losses incurred by reabsorption/re-emission events.⁴

In this study, we focus on the computational modeling of LSCs based on “type-II” semiconductor CdSe-CdTe nanoparticles.^{15–17} The computational results show that these semiconductor-based LSCs can be significantly more efficient and cost effective compared with current LSCs. The CdSe-CdTe nanoparticles have two main advantages compared with organic dyes (see Fig. 2): (i) A wider absorption band at shorter wavelengths; and (ii) a smaller reabsorption probability, making them less prone to losses due to multiple absorption-re-emission events. This is also a big advantage

over conventional single material semiconductor nanoparticles. In addition, the photoluminescence quantum yield of CdSe-type quantum dots (QDs) can be quite high (see Ref. 18 for quantum yields above 90%), while overcoating such QDs with a larger bandgap semiconductor has been shown to greatly increase the stability for use in LSCs.¹³

Besides the choice of particles, LSCs have several design parameters that can affect their performance. To analyze the performance of semiconductor-based LSCs in detail we employ Monte Carlo simulations (see Sec. II) using the measured data for CdSe-CdTe. The optimal particle concentration, loss mechanisms, and optimal LSC size are analyzed in Secs. III and IV. We find that such LSCs can be highly efficient. The optimal LSC gain is achieved with a PV cell covering a single edge and with a fairly long LSC box, i.e., the $l_x \approx 5l_y$, where l_x and l_y are the dimensions along the x and y axes (see Fig. 1).

A significant loss mechanism in LSCs is the escape of light from the top surface. In Sec. V we explore the use of CdSe-CdTe nanorods that are aligned perpendicular to the top surface. This design induces anisotropic luminescence with a preferred direction in the plane parallel to the top surface, thus reducing the escape of light from the LSC. We find that aligned nanorods can significantly increase the LSC gain compared with QDs. The computed maximal LSC gain is 7.6. These theoretical findings are encouraging for further research into semiconductor-based LSCs.

II. MONTE CARLO SIMULATIONS FOR PHOTON TRANSPORT

Monte Carlo (MC) simulations for photon transport (also called ray tracing) are a common tools for studying light propagation in random media when phase-dependent wave effects, such as interference and diffraction, are negligible.^{19,20} This approach is especially efficacious for light propagation in LSCs, because of the ability to incorporate multi-physics phenomena. Figure 3 depicts the MC algorithm we use.

^{a)}Author to whom correspondence should be addressed. Electronic mail: bilan@ucmerced.edu.

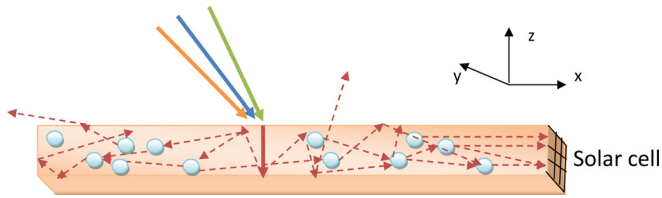


FIG. 1. (Color online) Illustration of light propagation in a LSC.

A photon is launched into the LSC and tracked until it is either lost due to radiation effects (not absorbed or reemitted), escapes from the LSC, or reaches the PV cell where it is collected (counted). We consider a box-shaped LSC (see Fig. 1) with dimensions $|x| \leq l_x$ (length, $2l_x$), $|y| \leq l_y$ (width, $2l_y$), and $|z| \leq l_z$ (thickness, $2l_z$). A PV cell is assumed to cover the right $y-z$ edge, i.e., $x = +l_x$ (see Sec. IV for the case of the PV cell covering all of the edges). Perfect mirrors are assumed to cover the bottom surface ($z = -l_z$) and on all the other edges. Therefore, light can only escape from the top surface.

To obtain statistically reliable results, we use at least 10^5 photons for each incident wavelength and the LSC parameters (particle concentration, LSC size, etc.). The algorithm is discussed in the following text in detail.

A. Absorption and emission

In general, the probability of a photon being absorbed after propagating a distance, Δs (in cm), is given by the Beer-Lambert law,²¹

$$p(\Delta s; \lambda) = 1 - 10^{-\epsilon(\lambda)M\Delta s}, \quad (1)$$

where M is the molar concentration of the particles (in mol/L) and $\epsilon(\lambda)$ is the extinction coefficient (in $L/\text{mol cm}$), which we obtain from the measured absorption spectrum (see Fig. 2).

Initially, a photon is launched at the center of the LSC's top surface at normal angle (see also Sec. VI for extensions), with a wavelength, λ , that is sampled randomly from the absorption spectrum. If the photon is not absorbed within a distance

$$\Delta s_0 = 2l_z, \quad (2)$$

where l_z is the LSC height, the photon is assumed to bounce from the bottom mirror at normal angle and then escape from

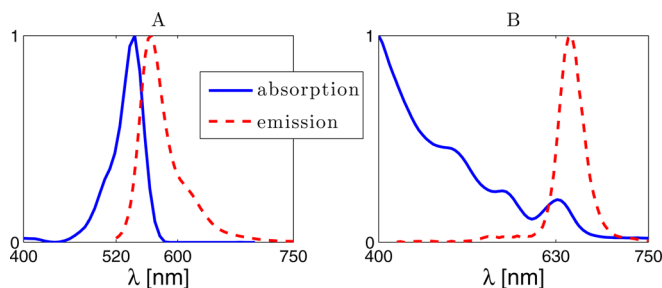


FIG. 2. (Color online) Normalized absorption (solid line) and emission (dashed line) spectra of (a) Rhodamine-B (an organic dye), and (b) Type II CdSe-CdTe quantum dots. The reabsorption probability depends on the overlap between the absorption and emission spectra, which is much smaller for the quantum dots.

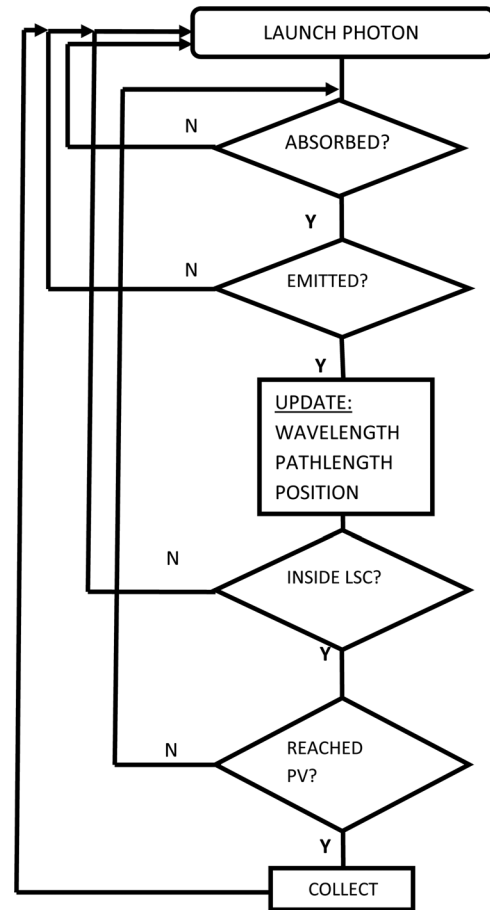


FIG. 3. Schematic representation of the MC algorithm.

the top surface (see Sec. II. B). In that case, the simulation resumes with a new photon. For subsequent reemission events a random path length is chosen by “solving” (1) to obtain

$$\Delta s = -\frac{1}{\epsilon(\lambda)M} \log_{10} \xi, \quad (3)$$

where, here and in what follows, ξ denotes a random variable that is uniformly distributed in $[0, 1]$.

If the photon is absorbed, it is reemitted only if,

$$\xi < QY, \quad (4)$$

where QY , the quantum yield, is the measured ratio of reemitted to absorbed photons.

If the photon is reemitted, its wavelength, position, and direction are updated as follows. The photon's new wavelength is sampled randomly from the normalized emission spectrum, as if the luminescence were memoryless. We note that for semiconductor particles, the assumption of completely memoryless luminescence overestimates the reabsorption losses from the second event. This is because when photons are (re)absorbed at the red edge of the absorption spectrum, they will more likely be reemitted further to the red due to inhomogeneous broadening, in which case they are less likely be reabsorbed again.

The photon's new position (x', y', z') is updated based on its incident direction as,

$$\begin{aligned}x' &= x + \mu_x \Delta s, \\y' &= y + \mu_y \Delta s, \\z' &= z + \mu_z \Delta s,\end{aligned}\quad (5)$$

where $(\mu_x, \mu_y,$ and $\mu_z)$ are the direction cosines and Δs is given by (3). The direction cosines themselves are updated in a two-step process. For isotropic QDs, the new azimuthal angle and cosine of the deflection angle are obtained using,

$$\varphi = 2\pi\xi \quad (6)$$

and

$$\cos \theta = \text{sign}(\chi) - \chi, \quad \chi \equiv 2\xi - 1, \quad (7)$$

so that $\phi \in [0, 2\pi)$, $\theta \in (0, \pi)$, and the reemitted light is isotropically distributed. Using (6) and (7) the direction cosines are then updated according to,

$$\mu'_x = \frac{\sin \theta}{\sqrt{1 - \mu_z^2}} (\mu_x \mu_z \cos \varphi - \mu_y \sin \varphi) + \mu_x \cos \theta, \quad (8a)$$

$$\mu'_y = \frac{\sin \theta}{\sqrt{1 - \mu_z^2}} (\mu_y \mu_z \cos \varphi + \mu_x \sin \varphi) + \mu_y \cos \theta, \quad (8b)$$

$$\mu'_z = -\sin \theta \cos \varphi \sqrt{1 - \mu_z^2} + \mu_z \cos \theta. \quad (8c)$$

Equations (8a)–(8c) correspond to luminescence at deflection angles (θ, φ) with respect to the incident radiation.¹⁹ If the incident direction is almost normal to the (x, y) plane, i.e., $|\mu_z| > 0.99999$, the direction cosines are updated using the asymptotic formulas for $|\mu_z| \rightarrow 1$, which are

$$\mu'_x = \sin \theta \cos \varphi, \quad (9a)$$

$$\mu'_y = \sin \theta \sin \varphi, \quad (9b)$$

$$\mu'_z = \sin(\mu_z) \cos \theta. \quad (9c)$$

See Eqs. (16) and (17) for the case of anisotropic luminescence.

B. LSC size and boundary conditions

LSCs are designed to reflect most of the light back from the top surface by using a medium with an index of refraction greater than 1. We assume $n_{\text{LSC}} = 1.7$, which allows for total internal reflection whenever $\mu_z < \mu_{\text{cr}} = \sin^{-1}(1/1.7) \approx 0.81$ (i.e., light is reflected when the incident angle is greater than 36° with respect to the zenith). When $\mu_z > \mu_{\text{cr}}$ the photon is assumed to reflect if

$$\xi < R(\beta), \quad \beta \equiv \cos^{-1}(\mu_z),$$

where $R(\beta)$ is the Fresnel reflection coefficient for unpolarized light.²² Otherwise, the photon escapes from the LSC.

When a photon arrives at the PV cell it is assumed to be collected. In reality, PV cells have a bandgap for the efficient conversion of light into electricity. In this regard, our computations yield an upper bound on the optical efficiency of the LSC (see Eq. 10). Nevertheless, these particles have a nar-

row emission band that falls well within the typical bandgap of PV cells.

C. Solar-averaged optical efficiency and LSC gain

A common metric for LSC performance is the optical efficiency, $\eta(\lambda)$, which is defined as the ratio of incident photons at wavelength, λ , to the collected photons (at any wavelength). A more relevant metric for the LSC performance is the solar-averaged optical efficiency,

$$\bar{\eta} = \frac{\int_{\lambda_{\min}}^{\lambda_{\max}} N_{\text{solar}}(\lambda) \eta(\lambda) d\lambda}{\int_{\lambda_{\min}}^{\lambda_{\max}} N_{\text{solar}}(\lambda) d\lambda}, \quad N_{\text{solar}}(\lambda) \doteq \frac{I_{\text{solar}}(\lambda)}{\lambda}, \quad (10)$$

where $I_{\text{solar}}(\lambda)$ is the solar irradiance at sea level, and $N_{\text{solar}}(\lambda)$ is proportional to the number of photons per area per wavelength. We obtain $I_{\text{solar}}(\lambda)$ from Ref. 23 and use $\lambda_{\min} = 400\text{nm}$ and $\lambda_{\max} = 750\text{nm}$. Thus, $\bar{\eta}$ is a measure of the ratio between the total photons collected by the PV cell and the total photons incident on the LSC.

The solar-averaged optical efficiency is an adequate metric of the LSC performance when the LSC dimensions are fixed. However, a more useful metric is the LSC gain,

$$\Gamma(\lambda) = \eta(\lambda) \times G, \quad (11)$$

and the solar-averaged LSC gain,

$$\bar{\Gamma} = \bar{\eta} \times G, \quad (12)$$

where G , the geometric factor, is the ratio of the area directly exposed to sunlight (the top surface area) to the area covered by the PV cell, i.e.,

$$G \equiv \frac{A_{\text{top}}}{A_{\text{PV}}}. \quad (13)$$

See Sec. IV for further details. The advantage of using the LSC gain is twofold:

1. The gain, $\bar{\Gamma}$, measures the ratio of collected photons using the LSC compared with exposing the (same) PV cell directly to the sun. As such, it must be (substantially) greater than 1 in order for the LSC to be cost-effective.
2. Unlike $\bar{\eta}$, which generally decreases with the LSC size, $\bar{\Gamma}$ attains its maximum value at some finite dimensions (see Fig. 8). This is useful for finding the optimal LSC dimensions.

We note that $\bar{\Gamma}$ serves as a lower bound on the actual gain, because the LSC can also capture diffuse light and also converts light into the PV bandgap.

III. OPTIMAL PARTICLE CONCENTRATION

A photon can undergo multiple absorption and re-emission events inside the LSC. The quantum yield, QY, is a measure of the emitted to absorbed photons. Light that is not reemitted is typically lost. For these CdSe-CdTe QDs, the QY = 95%. However, the probability of reemission diminishes quickly with the number of reabsorption-reemission events. Therefore, under ideal conditions, most photons should be

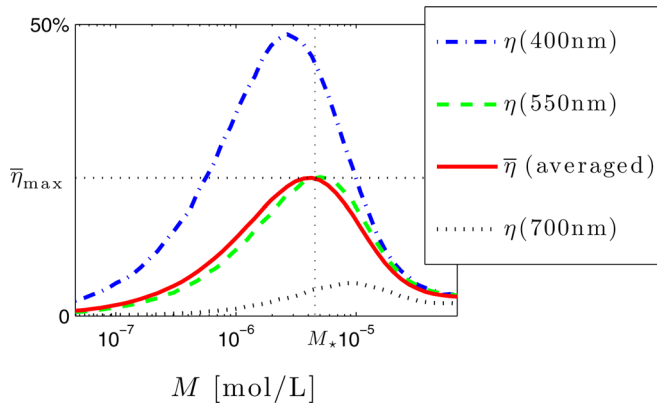


FIG. 4. (Color online) Solar-averaged optical efficiency $\bar{\eta}$ (solid line) and the wavelength-dependent optical efficiency for three different incident wavelengths (see legend) as functions of the quantum-dot concentration (log scale). A maximum optical efficiency of $\bar{\eta}_{\max} = 23.67\%$ is reached at $M_* = 4.3 \times 10^{-6} \text{ mol/L}$.

absorbed and reemitted once before being collected by the PV. Whether this happens depends on the particle concentration, M , in a complex way. The value of M that will maximize $\eta(\lambda)$ varies with λ . Therefore, we are interested in the optimal concentration that yields the maximum of $\bar{\eta}$ (Eq. 10).

Since the probability of absorption increases with the particle concentration [see Eq. (1)], the concentration should not be too high. On the contrary, the concentration should not be too low, lest the photons will not be absorbed at all. Hence, the optimal concentration must strike a balance between these competing loss mechanisms. However, there is more to the story, since the probability of reabsorption depends on the overlap between the absorption and emission spectra. In this regard, the small reabsorption of semiconductor nanoparticles is a key advantage. Therefore, by using semiconductor particles, a higher concentration can be chosen while keeping the reabsorption losses small.

To find the optimal concentration we fix the LSC dimensions as $l_x \times l_y \times l_z = 6 \text{ cm} \times 2 \text{ cm} \times 0.4 \text{ cm}$ and vary M between 10^{-8} and 10^{-5} mol/L . The maximum solar-averaged optical efficiency is

$$\bar{\eta}_{\max} \equiv \max_M(\bar{\eta}) \approx 24\%,$$

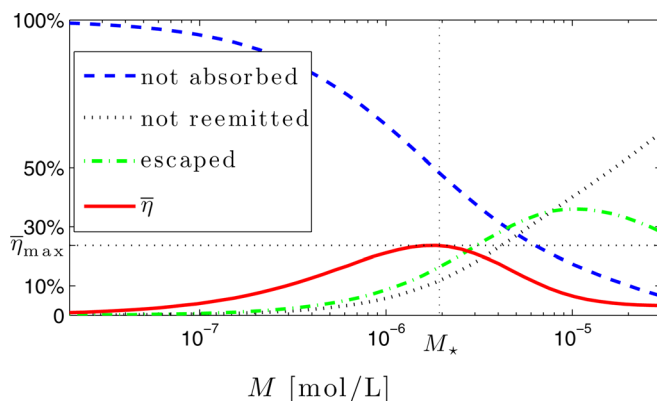


FIG. 5. (Color online) Dependence of the solar-averaged optical efficiency $\bar{\eta}$ (solid line), emission/reabsorption losses (dotted line), and escape from the top surface (dashed line) on the particle concentration.

which is achieved at $M = M_* \approx 4.3 \times 10^{-6} \text{ mol/L}$ (see Fig. 4). Figure 4 also shows that, if considering light incident at a particular wavelength, the optimal concentration generally increases somewhat with longer incident wavelengths. This is expected as $\epsilon(\lambda)$ mostly decreases with λ . The optimal concentration is also approximately the same as that which would be obtained using $\lambda = 630 \text{ nm}$ alone (see also Fig. 7).

Figure 5 shows the breakdown of the (statistically averaged) loss mechanisms and their dependence on particle concentration. As M increases, more photons are initially absorbed in the LSC. At the same time, more photons are lost, either due to not being reemitted (i.e., not emitted or not reabsorbed in the first or subsequent luminescence events) or due to photons escaping from the top surface. At the optimum, approximately 57% of the incident photons are not absorbed, the emission/reabsorption losses are 8.5%, and the escape loss is 12%.

Figure 6 shows that the collected spectrum is slightly shifted to the red compared with the single-emission spectrum. This tiny Stokes shift is due to the reabsorption, which peaks around 630 nm. To analyze this further, Fig. 7 shows that the reabsorption and escape losses have a local peak around 630 nm, as does the initial absorption (i.e., the not-absorbed curve has a dimple). As previously mentioned, at $M = M_*$ the solar-averaged efficiency $\bar{\eta}_{\max}$ is also about the same as $\eta(630 \text{ nm})$. Thus, the maximum solar-averaged efficiency, $\bar{\eta}_{\max}$, is achieved by balancing the competing loss mechanisms over the visible spectrum.

IV. OPTIMAL LSC SIZE

Thus far, the results were for fixed LSC size and assuming a PV cell that covers the right $y-z$ edge. It is interesting to study how the LSC performance changes with size and location of the PV cell. In general, as the area of the top surface of the LSC increases, more light enters the medium, but has a greater chance of being lost due to reabsorption or escape. The question arises as to what are the optimal LSC dimensions? To address this, the LSC gain [Eqs. (11) and (12)] serves as the most relevant performance metric.

We first assume (as before) that the PV cell covers the single edge, i.e., the right $y-z$ edge ($x = +l_x$). The single-edge geometric gain factor (13) is,

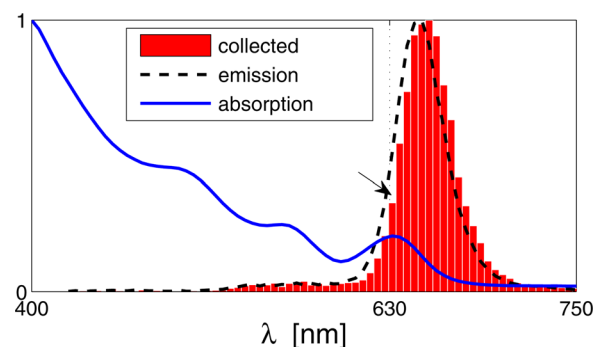


FIG. 6. (Color online) Same as Fig. 2(b) with the addition of the collected spectrum at the PV cell using $M = M_*$ (see Fig. 4). The arrow indicates a small Stokes shift ($\approx 5 \text{ nm}$) between the emission spectrum of the QDs (dashed line) and collected spectrum (histogram).

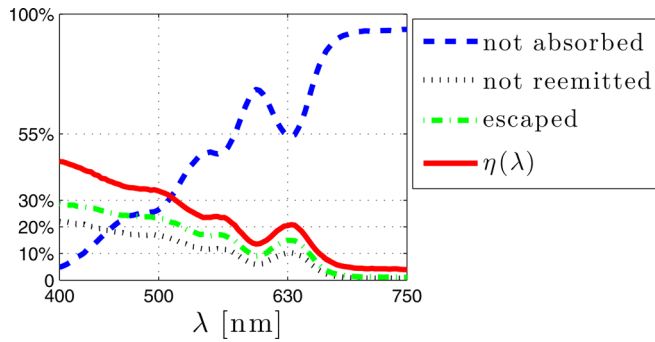


FIG. 7. (Color online) Same as in Fig. 5 showing the dependence of $\eta(\lambda)$ and the loss mechanisms on the incident wavelength, λ , with $M = M_*$.

$$G_{\text{single}} = \frac{A_{\text{top}}}{A_{\text{PV}}} = \frac{l_x l_y}{l_y l_z} = \frac{l_x}{l_z}. \quad (14)$$

We fix $l_y = 2\text{cm}$ and $l_z = 0.4\text{cm}$ and vary the LSC length, l_x . Therefore, the area covered by the PV cell remains constant, while the top surface area increases. Our computations show that the optimal LSC dimensions depend only weakly on the particle concentration and incident wavelength. For this reason, we initially fix $M = 4.3 \times 10^{-6}\text{mol/L}$ (M_* found previously for $l_x = 6\text{cm}$, $G_{\text{single}} = 15$) and use the incident light at $\lambda = 630\text{nm}$. Figure 8 presents the results. As the length, l_x , increases the optical efficiency decreases. This is not surprising, since a smaller fraction of the total incident photons arrives at the edge covered by the PV cell due to reabsorption and escape losses. What is, perhaps, more relevant is that the LSC gain peaks at $\bar{\Gamma} = 4$ when $G_{\text{single}} = 26$, which corresponds to $l_x/l_y = 5.2$, $l_x = 10.4\text{cm}$. Hence, the optimum performance is reached with a fairly long LSC box. This is also evident from Table I. Indeed, at the optimal LSC size ($G_{\text{single}} = 26$), the solar averaged efficiency is $\bar{\eta} = 13\%$, which is somewhat lower than 23.67% obtained using $G_{\text{single}} = 15$, yet the gain is a bit larger. Moreover, if a square LSC were to be used ($l_x = l_y = 2$, $G_{\text{single}} = 5$), then $\bar{\eta} \approx 37\%$ is even higher, however, the gain would be reduced by more than half compared with the optimum.

A related question is whether it is better to cover all the LSC edges with PV cells, i.e., on $|x| = l_x$ and $|y| = l_y$. Due to symmetry considerations, the optimal dimensions are achieved using a square LSC, $l_x = l_y$. At first thought, covering all the edges with PV cells might seem like a good idea because light has to travel a shorter distance to reach a PV cell, thereby reducing the reabsorption and escape losses.

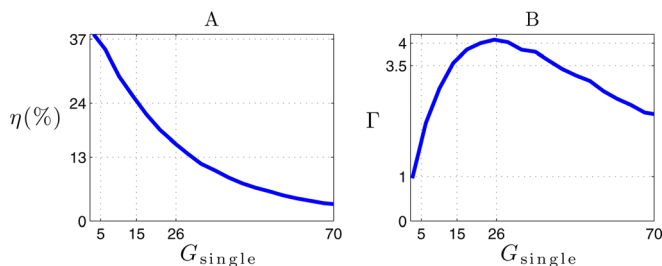


FIG. 8. (Color online) (a) Optical efficiency, η , and (b) LSC gain, Γ , at 630 nm as functions of the single-edge geometric factor (14).

TABLE I. Gain and loss characteristics using QDs for different LSC dimensions, when the PV cell covers the edge, $x = l_x$.

G_{single}	l_x/l_y	Not absorbed (%)	Not reemitted (%)	Escaped (%)	$\bar{\eta}$ (%)	$\bar{\Gamma}$
5	1	48	7	8	37	1.85
15	3	49	14	13	24	3.2
26	5.2	48	15	21	16	4

However, since in this case, $A_{\text{PV}} = 2(l_x + l_y) = 4l_x$, the all-edges geometric gain factor is only

$$G_{\text{all}} = \frac{l_x}{4l_z} = \frac{1}{4} \times G_{\text{single}}. \quad (15)$$

In fact, our computations show that when all of the LSC edges are covered with PV cells, $\bar{\Gamma}_{\text{max}}$ is only marginally greater than 1 (see Table II). In this vein, we remark that, under the condition of optimal particle concentration, most photons are absorbed and reemitted only once, which is an advantage due to the small reabsorption cross-section of these QDs. The reemitted light rays bounce back and forth, impinging on the top surface at the same (or more grazing and hence, more reflecting) angle each time, until they reach the edge covered by a PV cell. Indeed, as the geometric factor increases, the fraction of light flux that is not reemitted or escapes grows at a much slower rate (see Tables I and II). Taking into account the cost of the extra PV material needed compared with a single-edge PV cell, we conclude that a single-edge PV cell is a much more cost-effective design.

V. ANISOTROPIC LUMINESCENCE

As shown in Table I, under optimal conditions almost 20% of the light escapes from the LSC. While this can be mitigated using special coatings and filters (cf., Refs. 24 and 25), the escape of light from the LSC remains a significant loss mechanism. In order to ameliorate this, we investigate using aligned semiconductor nanorods, i.e., rod-shaped CdSe-CdTe nanoparticles that are aligned in the LSC with their long axis perpendicular to the top surface (see Fig. 9). This induces anisotropic luminescence that peaks in the plane parallel to the top surface, thus reducing the escape of light from the LSC. Similar approaches have recently been studied for dye-based LSCs.^{26–30}

One of the advantages of semiconductor nanorods compared with dyes is that, when semiconductor nanorods are aligned and cannot rotate, their luminescence is polarized, while their absorption is approximately isotropic.^{31–33} This

TABLE II. Same as Table I when the PV cells cover all the edges of a square LSC.

G_{all}	$l_x = l_y$	Not absorbed (%)	Not reemitted (%)	Escaped (%)	$\bar{\eta}$ (%)	$\bar{\Gamma}$
5.4	8.6	48.4	12.1	16.2	23.3	1.25
15	3	49	14	13	24	3.2
15	24	48.5	18.2	25.2	8.1	1.21

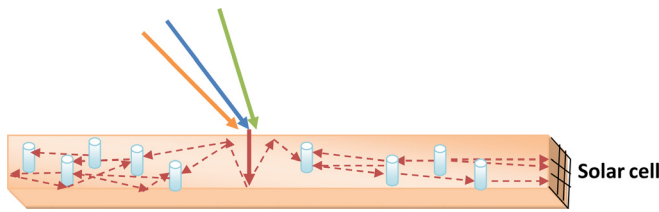


FIG. 9. (Color online) Light propagation in a LSC with aligned nanorods.

is due to their electronic structure. Specifically, for single-material nanorods (CdSe or CdTe), the transition from the top of the valence band to the bottom of the conduction band is polarized along the long axis of the nanorods. However, at higher energies, there is a high density of transitions that are polarized both along and normal to the nanorod axis. The net effect is that, except at the red edge of the spectrum, the absorption is approximately isotropic. The same is true of CdSe/CdTe nanorods that form a type-II heterojunction.^{34–36} In that case, the luminescence is from a charge transfer transition, which is also polarized along the nanorod long axis.

For aligned nanorods we assume isotropic absorption. However, instead of using (8), the direction of the reemitted photon is given by,

$$\mu'_x = \sin \theta \cos \varphi, \mu'_y = \sin \theta \sin \varphi, \mu'_z = \cos \theta, \quad (16)$$

where, in this case, $\theta \in [0, \pi)$ is the absolute luminescence angle with respect to the zenith. To compute θ , we use the inverted the Henyey-Greenstein formula for anisotropic luminescence,¹⁹

$$\cos \theta = \text{sign}(\chi) - \chi, \quad (17)$$

$$\chi \equiv \frac{1}{2g} \left[1 + g^2 - \left(\frac{1 - g^2}{1 + 2g\xi - g^2} \right)^2 \right],$$

where g is the anisotropy coefficient. The limit, $g \rightarrow 0$, gives the isotropic luminescence. When $g = 1$, Eq. (17) gives $\theta = \pi/2$, which corresponds to luminescence only in the

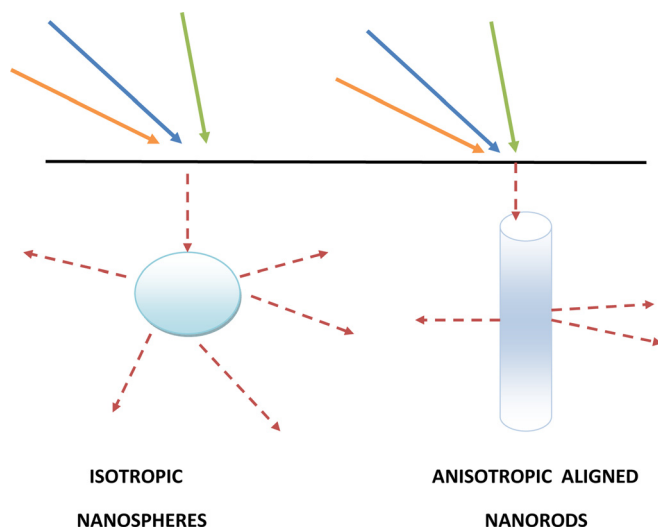
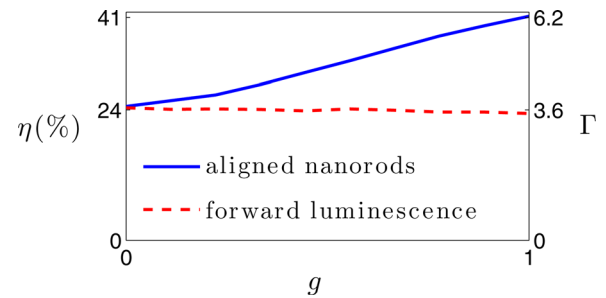


FIG. 10. (Color online) Illustration of forward luminescence by spherical quantum dots and anisotropic luminescence by aligned nanorods.

FIG. 11. (Color online) Optical efficiency (left axis) and LSC gain (right axis) for $\lambda = 630\text{nm}$ based on anisotropic luminescence of aligned nanorods (solid line) vs forward luminescence (dashed line) as functions of the anisotropy parameter, g [Eq. (17)].

plane parallel to the top surface. Any other value of $0 < g < 1$ corresponds to conical luminescence relative to the (x, y) plane.

Fixing the LSC dimensions with $l_x = 6\text{cm}$, $l_y = 2\text{cm}$, $l_z = 0.4\text{cm}$, using $\lambda = 630\text{nm}$ and $M = 5.8 \times 10^{-6}\text{mol/L}$ (see the following text), we compute the optical efficiency and LSC gain as a function of the anisotropy, g . Figure 11 shows that the LSC performance increases monotonically with g . For $g \approx 1$, with aligned nanorods, the LSC gain is more than 70% higher compared with using isotropic QDs.

For comparison, we also consider forward conical luminescence (see Fig. 10). This would be the case, for example, for spherical quantum dots or anisotropic nanorods that are randomly oriented in the LSC. In the latter case, the luminescence would peak in the same direction as the absorbed light, but since the particles are randomly aligned, on average, their luminescence would be in a random direction. To model this computationally, we revert to (8), but with the cosine of the deflection angle (with respect to the incident direction of light) given by (17). Figure 11 shows that, not surprisingly, the results are almost the same as using isotropic QDs. Hence, achieving well-aligned nanorods is important.

Figure 12 shows the loss mechanisms using aligned nanorods with $g = 0.95$. In comparison with Fig. 5, the most significant difference is that almost no light escapes from the LSC. Consequently, the optimal particle concentration is somewhat higher than for isotropic QDs.

Table III presents a comparison of the LSC performance metrics using aligned nanorods with $g = 0.95$ for different

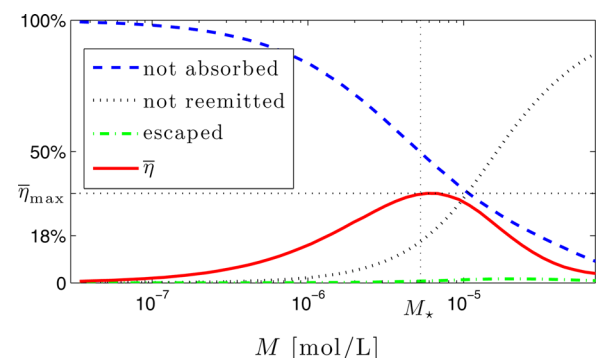
FIG. 12. (Color online) Same as Fig. 5 using aligned nanorods with $g = 0.95$.

TABLE III. Same as Table I for LSCs with aligned nanorods and $g = 0.95$.

G	l_x/l_y	Not absorbed (%)	Not reemitted (%)	Escaped (%)	$\bar{\eta}$ (%)	$\bar{\Gamma}$
5	1	54.4	5.9	0.2	39.5	1.97
15	3	37.5	21.3	0.9	40.3	6
25	5	47	24	1.1	27.9	7.6

LSC dimensions for the same l_y and l_z used for Table I and the PV on a single edge. Once again, the optimal dimensions are approximately $l_x : l_y = 5 : 1$. However, in this case, the maximal solar-averaged gain is 7.6.

VI. SPATIAL AND ANGULAR DISTRIBUTIONS OF THE INCIDENT LIGHT

The results in the previous text assumed that light is incident at the center of the top surface, at normal angle to the surface, and is transmitted into the LSC with probability 1. In this section we study the dependence of the gain on the spatial and angular distribution of the incident light.

In general, light incident closer to the edge covered by the PV cell has a greater collection probability and light that is incident on the opposite edge has a smaller collection probability. This is demonstrated in Fig. 13, where the PV cell is at $x_0 = l_x = 10$. This figure shows that light that is incident on the opposite edge ($x_0 = -10$) has almost the same chance of collection as light incident at the center of the top surface ($x_0 = 0$). This is because: (i) the reemitted light has a fairly small chance of being reabsorbed, and (ii) if the reemitted light reflects from the top surface (back into the LSC) once, it is very likely to reflect in all the subsequent scatterings from the top surface. Since sunlight impinges on the LSC surface with an almost spatially uniform radiant intensity, the results obtained in the previous sections by assuming that light is incident at the center of the top surface yield a lower bound on the LSC performance.

Figure 14(a) shows the dependence of the Fresnel transmission coefficient for light incident on the top surface as a function of the angle of incidence (with respect to the ze-

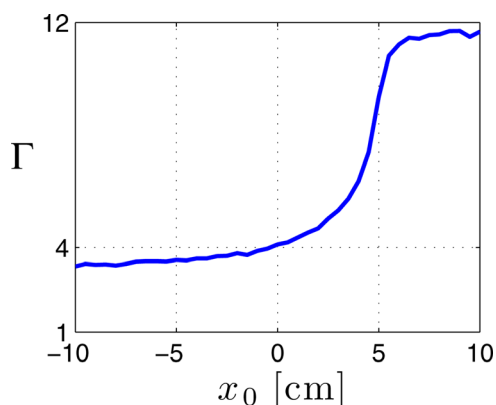


FIG. 13. (Color online) Dependence of gain on the location of the incident light along the length of the LSC. The PV cell covers the $y-z$ edge at $x = 10$.

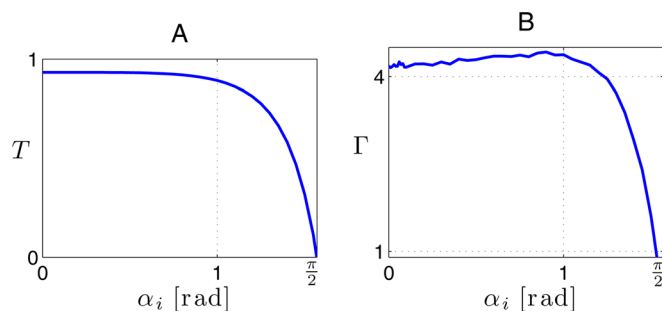


FIG. 14. (Color online) (a) Transmission coefficient, and (b) gain as functions of the incident angle.

nith). For angles below 1 rad, almost all of the light is transmitted into the LSC. Figure 14(b) shows the dependence of the gain on the angle of incidence, taking into account the transmission coefficient and generalizing (2) to include the transmission angle as,

$$\Delta s_0 = \frac{2l_z}{\cos(\alpha_t)}, \quad (18)$$

where α_i and α_t are related via Snell's Law. Equation (18) implies that light initially travels a greater distance as the incident angle increases (becomes more grazing), thereby decreasing the initial losses due to escape. Furthermore, Fig. 14(b) shows that, for light that is incident in a cone with an opening half-angle of 1 rad from the zenith, the gain is approximately the same as at normal incidence ($\alpha_i = 0$). Since most of the diurnal irradiance falls within this cone, the results obtained in previous sections by assuming that the light is incident at a normal angle to the surface yield a very good approximation of the diurnal LSC performance.

VII. CONCLUSIONS

The results of the computations in this study suggest that LSCs based on CdSe-CdTe quantum dots can be more efficient than current LSC designs. Moreover, using aligned nanorods can increase the LSC performance by 70% compared with using quantum dots. The maximal LSC gain of 7.6 (Table III) implies that such LSCs can be that much more efficient compared with exposing the PV cell directly to the sun and even more so, since LSCs can also collect diffuse light. These theoretical findings are encouraging for further research into semiconductor-based LSCs.

ACKNOWLEDGMENTS

We thank Xichen Cai and Hoda Mirafzal for sharing their measured data of CdSe-CdTe nanoparticles. This research is supported by the Natural Science Foundation SOLAR Program under Grant No. CHE-0934615.

¹W. H. Weber and J. Lambe, *Appl. Opt.* **15**, 2299 (1976).

²A. Goetzberger and W. Greubel, *J. Appl. Phys.* **14**, 123 (1977).

³J. S. Batchelder, A. H. Zewail, and T. Cole, *Appl. Opt.* **18**, 3090 (1979).

⁴R. W. Olson, F. L. Roger, and M. D. Fayer, *Appl. Opt.* **20**, 2934 (1981).

⁵W. G. Van Sark, K. W. Barnham, L. H. Slooff, A. J. Chatten, A. Büchtemann, A. Meyer, S. J. McCormack, R. Koole, D. J. Farrell, R. Bose, E. E.

- Bende, A. R. Burgers, T. Budel, J. Quilitz, M. Kennedy, T. Meyer, S. H. Wadman, G. P. van Klink, G. van Koten, A. Meijerink, and D. Vanmaekelbergh, *Opt. Express* **16**, 21773 (2008).
- ⁶B. Rowan, L. Wilson, and B. Richards, *IEEE J. Sel. Top. Quantum Electron.* **14**, 1312 (2008).
- ⁷M. J. Currie, J. K. Mapel, T. D. Heidel, S. Goffri, and M. A. Baldo, *Science* **321**, 226 (2008).
- ⁸J. C. Goldschmidt, M. Peters, A. Bösch, H. Helmers, F. Dimroth, S. W. Glunz, and G. Willeke, *Solar Energy Mater. Sol. Cells* **93**, 176 (2009).
- ⁹L. H. Slooff, E. E. Bende, A. R. Burgers, T. Budel, M. Pravettoni, R. P. Kenny, E. D. Dunlop, and A. Büchtemann, *Phys. Status Solidi (RRL)* **2**, 257 (2008).
- ¹⁰S. Tsoi, D. J. Broer, C. W. Bastiaansen, and M. G. Debije, *Opt. Express* **18**, A536 (2010).
- ¹¹A. Chatten, K. Barnham, B. Buxton, N. Ekins-Daukes, and M. Malik, *Semiconductors* **38**, 909 (2004).
- ¹²V. Sholin, J. D. Olson, and S. A. Carter, *J. Appl. Phys.* **101**, 123114 (2007).
- ¹³M. G. Hyldahl, S. T. Baileya, and B. P. Wittmershaus, *Sol. Energy* **83**, 566 (2009).
- ¹⁴G. V. Shcherbatyuk, R. H. Inman, C. Wang, R. Winston, and S. Ghosh, *Appl. Phys. Lett.* **96**, 191901 (2010).
- ¹⁵S. Kim, B. Fisher, H.-J. Eisler, and M. Bawendi, *J. Am. Chem. Soc.* **125**, 11466 (2003).
- ¹⁶C.-H. Chuang, S. S. Lo, G. D. Scholes, and C. Burda, *Phys. Chem. Lett.* **1**, 2530 (2010).
- ¹⁷T. Ju, L. Yang, and S. Carter, *J. Appl. Phys.* **107**, 104311 (2010).
- ¹⁸X. Cai, H. Mirafzal, and D. F. Kelley (unpublished).
- ¹⁹S. A. Prahl, M. Keizer, S. L. Jacques, and A. J. Welch, *SPIE Inst. Ser.* **IS**, 102 (1989).
- ²⁰L. Wang and H. Wu, *Biomedical Optics: Principles And Imaging* (Wiley, New York, 2007).
- ²¹W. Yu, L. Qu, W. Guo, and X. Peng, *Chem. Mater.* **15**, 2854 (2003).
- ²²M. Born and E. Wolf, *Principles of Optics: Electromagnetic Theory of Propagation, Interference and Diffraction of Light*, 7th ed. (Cambridge University Press, Cambridge, England, 2005).
- ²³K. Emery, *Reference Solar Spectral Irradiance, Technical Report*, ASTM, <http://rredc.nrel.gov/solar/spectra/am1.5>, 2000.
- ²⁴M. Kennedy, S. McCormack, J. Doran, and B. Norton, *Proc. SPIE* **6649**, 664905 (2007).
- ²⁵M. G. Debije, M.-P. Van, P. P. C. Verbunt, M. J. Kastelijn, R. H. L. van der Blom, D. J. Broer, and C. W. M. Bastiaansen, *Appl. Opt.* **49**, 745 (2010).
- ²⁶P. P. C. Verbunt, A. Kaiser, K. Hermans, C. W. M. Bastiaansen, D. J. Broer, and M. G. Debije, *Adv. Funct. Mater.* **19**, 2714 (2009).
- ²⁷C. L. Mulder, P. D. Reusswig, A. M. Velázquez, H. Kim, C. Rotschild, and M. A. Baldo, *Opt. Express* **18**, A79 (2010).
- ²⁸C. L. Mulder, P. D. Reusswig, A. P. Beyler, H. Kim, C. Rotschild, and M. A. Baldo, *Opt. Express* **18**, A91 (2010).
- ²⁹S. McDowall, B. L. Johnson, and D. L. Patrick, *J. Appl. Phys.* **108**, 053508 (2010).
- ³⁰R. W. MacQueen, Y. Y. Cheng, R. G. C. R. Clady, and T. W. Schmidt, *Opt. Express* **18**, A161 (2010).
- ³¹J. Hu, L.-S. Li, W. Yang, L. Manna, L.-W. Wang, and A. P. Alivisatos, *Science* **292**, 2060 (2001).
- ³²J. Hu, Wang, L.-S. Li, W. Yang, and A. P. Alivisatos, *J. Phys. Chem. B* **106**, 2447 (2002).
- ³³A. Shabaev and A. L. Efros, *Nano Lett.* **4**, 1821 (2004).
- ³⁴F. Shieh, A. E. Saunders, and B. A. Korgel, *J. Phys. Chem. B* **109**, 8538 (2005).
- ³⁵M. Jones, S. Kumar, S. S. Lo, and G. D. Scholes, *J. Phys. Chem. C* **112**, 5423 (2008).
- ³⁶L. Xi, C. Boothroyd, and Y. M. Lam, *Chem. Mater.* **21**, 1465 (2009).